MNRAS **000**, 1–12 (2015) Preprint 16 November 2015 Compiled using MNRAS LATEX style file v3.0

DIVE in the cosmic web: voids with Delaunay Triangulation from discrete matter tracer distributions

Cheng Zhao[1⋆], Charling Tao[2,1], Yu Liang[1], Francisco-Shu Kitaura[3] & Chia-Hsun Chuang[3]

[1] *Tsinghua Center for Astrophysics (THCA) & Department of Physics, Tsinghua University, Beijing 100084, China*
[2] *CPPM, Université Aix-Marseille, CNRS/IN2P3, Case 907, 13288 Marseille Cedex 9, France*
[3] *Leibniz-Institut für Astrophysik Potsdam (AIP), An der Sternwarte 16, D-14482 Potsdam, Germany*

arXiv:1511.04299v1 [astro-ph.CO] 13 Nov 2015

16 November 2015

ABSTRACT

We present a novel parameter-free cosmological void finder (DIVE, Delaunay TrIangulation Void findEr) based on Delaunay Triangulation (DT), which efficiently computes the empty spheres constrained by a discrete set of tracers. We define the spheres as DT voids, and describe their properties, including an universal density profile together with an intrinsic scatter. We apply this technique on 100 halo catalogues with volumes of $2.5\,h^{-1}$Gpc side each, with a bias and number density similar to the BOSS CMASS Luminous Red Galaxies, performed with the PATCHY code. Our results show that there are two main species of DT voids, which can be characterised by the radius: they have different responses to halo redshift space distortions, to number density of tracers, and reside in different dark matter environments. Based on dynamical arguments using the tidal field tensor, we demonstrate that large DT voids are hosted in expanding regions, whereas the haloes used to construct them reside in collapsing ones. Our approach is therefore able to efficiently determine the troughs of the density field from galaxy surveys, and can be used to study their clustering. We further study the power spectra of DT voids, and find that the bias of the two populations are different, demonstrating that the small DT voids are essentially tracers of groups of haloes.

Key words: methods: data analysis – catalogues – galaxies: structure – (*cosmology:*) large-scale structure of Universe

1 INTRODUCTION

Cosmic voids are large regions in space which contain only low luminosity (mass) galaxies (haloes/dark matter). Due to the low density nature of voids, they are less affected by non-linear gravitational effects, and thus should be less evolved, closer to the initial gaussian field of the universe (cf. e.g. van de Weygaert & van Kampen 1993; Sheth & van de Weygaert 2004). Therefore, voids are powerful tracers for cosmic structure formation and cosmological parameter constraints (e.g. Betancort-Rijo et al. 2009; Sutter et al. 2014), probing the nature of dark energy or alternate theories of gravity (e.g. Lee & Park 2009; Cai et al. 2015), and tests of the primordial non-Gaussianities (e.g. Song & Lee 2009). Moreover, in our companion papers Kitaura et al. and Liang et al., we show that voids present evidence of Baryon Acoustic Oscillations (BAO) signal, which provides additional information than that of galaxies, and is used as a standard ruler for measuring the distance of the Universe.

Voids can be defined in many different ways, suited for different purposes,

(i) under-dense regions based on the smoothed dark matter (or halo/galaxy) density field (Colberg et al. 2005; Shandarin et al. 2006; Platen et al. 2007; Neyrinck 2008);
(ii) gravitationally expanding regions based on the dynamics of the dark matter density field (Hahn et al. 2007; Forero-Romero et al. 2009; Hoffman et al. 2012; Cautun et al. 2013);
(iii) regions free of shell crossings based on phase-space tesselations of the particle distribution (Abel et al. 2012; Falck et al. 2012; Shandarin et al. 2012);
(iv) or empty spatial regions among discrete tracers (e.g. El-Ad & Piran 1997; Aikio & Mähönen 1998; Hoyle & Vogeley 2002; Padilla et al. 2005; Patiri et al. 2006; Foster & Nelson 2009).

The first three classes of methods require accurate esti-

⋆ E-mail: c-zhao15@mails.tsinghua.edu.cn

© 2015 The Authors

mates of the continuous density field and are thus not optimally suited for biased discrete tracers. We will focus for this reason in this work on the last class of methods, and present a new void finding algorithm (DIVE) based on the Delaunay Triangulation (DT, Delaunay 1934) technique, which generates meshes to discretise a spatial domain. DT is a powerful and popular tool in finite element analysis, with a variety of applications in computational geometry, geology (e.g. Braun et al. 2008), biology (e.g. Medek, Beneš & Sochor 2007), etc. In the past two decades, DT-based tools have been extensively exploited in astronomy (e.g. Bernardeau 1996; Marinoni et al. 2002; Pál & Bakos 2006; Cardiel et al. 2011; van de Weygaert et al. 2011; Bergé et al. 2012; Cedrés et al. 2012). In particular, Schaap & van de Weygaert (2000) developed the Delaunay Tessellation Field Estimator (DTFE) method for the reconstruction of a continuous density field from a set of discrete samples, which leads to many studies on the large-scale structures of the universe, from both theory and observation aspects (cf. e.g. Aragón-Calvo et al. 2007; Romano-Díaz & van de Weygaert 2007; van de Weygaert & Schaap 2007; Platen et al. 2011; Sousbie 2011; Jennings 2012).

As a geometric tool, the DT technique is naturally useful in cosmological studies, especially for cosmic voids: 1) it is parameter-free; 2) it is able to handle arbitrary shapes of domains, even with masked regions inside, which is generally the case for observations; 3) it can be very efficient with a large number of objects. Indeed, the Watershed Void Finder (WVF, Platen et al. 2007, based on DTFE) and ZOBOV (Neyrinck 2008, based on Voronoi Diagram, the dual graph of DT) void finders are both related to the DT technique. These two methods both focus on resolving voids from the underlying density field, while our method simply takes the circumsphere of triangulation cells from a set of discrete samples (i.e., galaxy or halo catalogues). As a direct product of the DT technique, we obtain the spherical regions, which we name "DT voids".

In section 2 we begin with a description of our void finding algorithm, and applied it to mock catalogues in section 3. Later, we present the properties of DT voids in section 4. Then, we study the dark matter in and around voids in section 5, and void clustering in section 6. Finally, we conclude in section 7 with a discussion on future studies.

2 THE DIVE ALGORITHM

In this section we present our approach based on the Delaunay triangulation, which emerges as a natural solution to define cosmic voids from discrete distributions of objects. We dub our method DIVE: **D**elaunay tr**I**angulation **V**oid find**E**r.

We consider the general case of a set P of points in d-dimensional Euclidean space E^d. The Delaunay Triangulation is a partition of the convex hull of P into a set T of d-simplices (triangles in 2-D space), whose vertices are points of P, and the circum-hyperspheres $\mathcal{C}(T)$ do not contain any of the points in P in their interiors.

In the 3-D case, DT defines all the empty spheres: $S \equiv \mathcal{C}(T)$, through the associated tetrahedra: T (the corresponding 3-D simplices), with the properties, also known as the Delaunay condition:

$$\forall\, t \in T, \quad \mathcal{V}(t) \subseteq P \tag{1}$$

$$\forall\, s \in S, \quad s^\circ \cap P = \varnothing, \tag{2}$$

where $\mathcal{V}(t)$ denotes the vertices of t, and $^\circ$ is the interior operator.

Within the cosmological context, the set P can be any kind of 3-D distribution of matter tracers, such as dark matter particles, haloes, galaxies, or quasars. In particular, we consider in this work the partition of haloes into tetrahedra, which circumspheres we call "DT voids".

Note that we do not assume that cosmological voids are spherical. In our case, DT voids do not represent individual empty regions. Instead, the distribution of DT void centres (which do not have to reside inside the associated tetrahedra) and radii associated to the corresponding circumspheres defined by tetrahedra, can be used to trace the space devoid of gravitationally collapsed objects (above certain luminosity or mass threshold).

As mentioned above, there is a deep relation between the Delaunay and the Voronoi Diagram. In fact connecting the centres of the circumspheres produces the Voronoi diagram (we refer to e.g. Icke & van de Weygaert 1987; Springel 2010; Lang et al. 2015, for applications of Voronoi Diagrams in cosmology).

The Delaunay Triangulation scheme to find all tetrahedra which connect all the N_P points (matter tracers in our case) proceeds by incremental construction: the vertices of tetrahedra are added one by one, together with reconfigurations of the affected tetrahedra to ensure that the Delaunay condition is fulfilled (i.e. the requirement that the circumspheres of all tetrahedra have empty interiors.). The vertices are added in a random order to reach the efficiency of $\mathcal{O}(N_P \log N_P)$.

In practice, we rely on the publicly available Computational Geometry Algorithms Library[1] (CGAL, Brönnimann, Fabri, Giezeman, Hert, Hoffmann, Kettner, Pion & Schirra 2015; Jamin, Pion & Teillaud 2015) to perform Delaunay Triangulation and compute the centre and radius of the circumsphere of tetrahedra based on the halo catalogues described in the next section.

Furthermore, the DIVE algorithm has been used in Kitaura et al. and Liang et al. to validate the methodology for BAO detection from voids, and applied to observations and large sets of mock catalogues to estimate the uncertainties on such measurements.

3 DIVE ON HALO CATALOGUES

To investigate the performance of the DIVE algorithm and properties of the cosmic DT voids we make use of large cosmological halo catalogues, which can be considered as proxies for Luminous Red Galaxy (LRG) catalogues, described below in §3.1, then we give a qualitative evaluation of the outcome of DIVE.

[1] http://www.cgal.org

3.1 Halo catalogues

In our study, the mock halo catalogues together with the associated dark matter density field were constructed with the PerturbAtion Theory Catalogue generator of Halo and galaxY distributions (the PATCHY-code, Kitaura et al. 2014).

In particular, we use the public input parameters of PATCHY (Kitaura et al. 2015b), which has been calibrated with the Spherical Overdensity (SO) halo catalogue (including sub-structures) of the BigMultiDark N-body simulations (Klypin et al. 2014) at redshift $z = 0.56$, within the framework of the Planck ΛCDM cosmology with $\{\Omega_{\rm M} = 0.307115, \Omega_b = 0.048206, \sigma_8 = 0.8288, n_s = 0.96\}$, and the Hubble parameter $H_0 \equiv 100\,h\,{\rm km\,s^{-1}Mpc^{-1}}$ given by $h = 0.6777$. The side length of the simulation box is $2.5\,h^{-1}$Gpc, and the grid size 960^3 (i.e., 960^3 dark matter particles). Nevertheless, only the dark matter field (based on augmented Lagrangian perturbation theory: ALPT, Kitaura & Heß 2013) on a mesh with resolution 2.6 h^{-1} Mpc is taken and the haloes are populated following the explicit Eulerian nonlinear and stochastic bias prescriptions in the PATCHY-code, permitting an accurate description of the clustering obtained with the reference N-body simulation using 3840^3 particles.

In fact, for the number density of haloes of around $3.5 \times 10^{-4}\,h^3\,{\rm Mpc}^{-3}$ used in this study, which is the typical density of LRG for the Baryon Oscillation Spectroscopic Survey[2] (BOSS, Eisenstein et al. 2011; Dawson et al. 2013), it has been demonstrated that the two and three-point statistics are accurately matched (cf. Chuang et al. 2015; Zhao et al. 2015). Furthermore, these halo catalogues can be used to construct realistic mock galaxy catalogues with the Halo Abundance Matching scheme (Kitaura et al. 2015a; Rodríguez-Torres et al. 2015).

We have generated 100 realisations of PATCHY mocks using the same input parameters with different seed initial conditions, to estimate the effects of cosmic variance in our analysis. Furthermore, we convert the PATCHY mocks to redshift space with the distant observer approximation, to study the performance in observed redshift space.

3.2 Numerical performance

We apply DIVE to the PATCHY halo catalogues containing about 5.5 million haloes each, and find that the Delaunay triangulation operations take on average ~ 6 minutes with a single CPU core. In order to ensure periodic boundary conditions, we expand the boxes by duplicating haloes beyond the box boundaries. The expansion length is chosen to be slightly larger than the radius of the largest void in the box. We then remove voids with centres outside the box to obtain the final DT void catalogue. This full procedure takes on average $\sim$10 minutes for one realisation using a single CPU core, which makes the DIVE algorithm suitable for the analysis of large data sets. Given the low memory requirement ($\mathcal{O}(N_P)$), the DIVE algorithm can be trivially applied in parallel to different catalogues, such as the 100 considered in this study.

[2] http://www.sdss3.org/surveys/boss.php

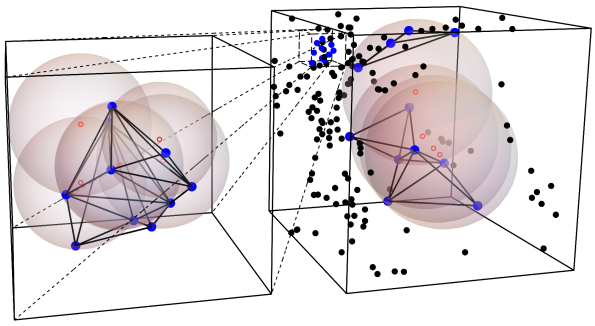

Figure 1. Part of the voids resolved in a halo catalogue (black and blue points), with an extensive radius range, recognised by the DIVE technique. The red open circles denote the centres of voids, and the blue points joint by solid lines (edge of the tetrahedra) indicate the haloes associated with the voids. *Left*: voids ($R_V \leqslant 4\,h^{-1}$Mpc) in a box with $12^3\,h^{-3}{\rm Mpc}^3$ volume. *Right*: voids ($R_V \in [26, 27]\,h^{-1}$Mpc) in a box with $80^3\,h^{-3}{\rm Mpc}^3$ volume.

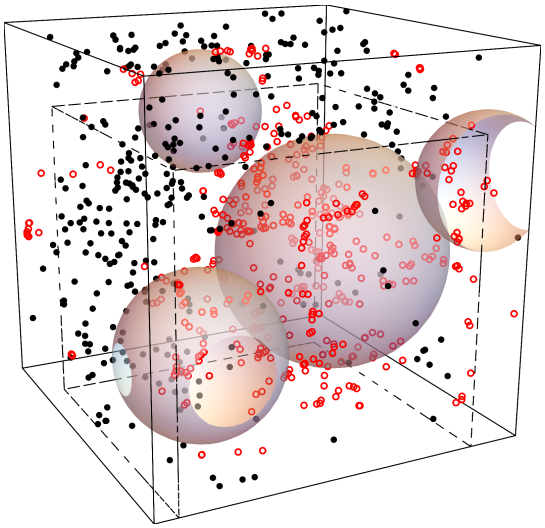

Figure 2. Maximum *disjoint voids* ($R_V \geqslant 17\,h^{-1}$Mpc) in a box with $100^3\,h^{-3}{\rm Mpc}^3$ volume. The red open circles indicate the centres of all the DT voids with the same radius cut. The dashed cube represents the box in the right hand side of Fig. 1.

3.3 Visualisations

The performance of DIVE applied to one PATCHY halo catalogue is illustrated in Fig. 1 and Fig. 2. From Fig. 1 we see that the centres of large voids (see the void radii of $R_V \geqslant 26\,h^{-1}$Mpc in Fig. 1) can be distantly located to the associated tetrahedra, which indicates that they reside in low halo number density regions, while this is not the case for very small voids (see the void radii of $R_V \leqslant 4\,h^{-1}$Mpc in Fig. 1). Fig. 2 shows that DIVE finds a large number of voids from a comparable or even smaller amount of halo tracers. This large number opens the possibility of using DT voids for clustering analyses.

3.4 Disjoint voids

As mentioned in the introduction, different definitions of voids can serve different purposes. DIVE can be straightforwardly applied to obtain another type of voids, the so-called maximum non-overlapping spheres (Patiri et al. 2006), which have been applied to study galaxy orientation (Trujillo et al. 2006; Brunino et al. 2007) and proposed to constraint cosmological parameters (Betancort-Rijo et al. 2009). These non-overlapping spheres can be obtained from the DT voids by sorting them in decreasing radius, and sequently removing overlapping voids. The shaded spheres in Fig. 2 show the disjoint spherical voids found by this post-processing procedure on the DT void catalogues.

From a hierarchical perspective, the *disjoint voids* can be regarded as distinct (parent) nodes, and the removed overlapping DT voids as the sub-structures in concordance with the hierarchical picture of voids discussed in previous works (cf. Sheth & van de Weygaert 2004, and references therein). Throughout this work we refer to these two populations (or definitions) of DT voids as: *all voids* and *disjoint voids*. Let us investigate more quantitatively the performance of DIVE in the coming section.

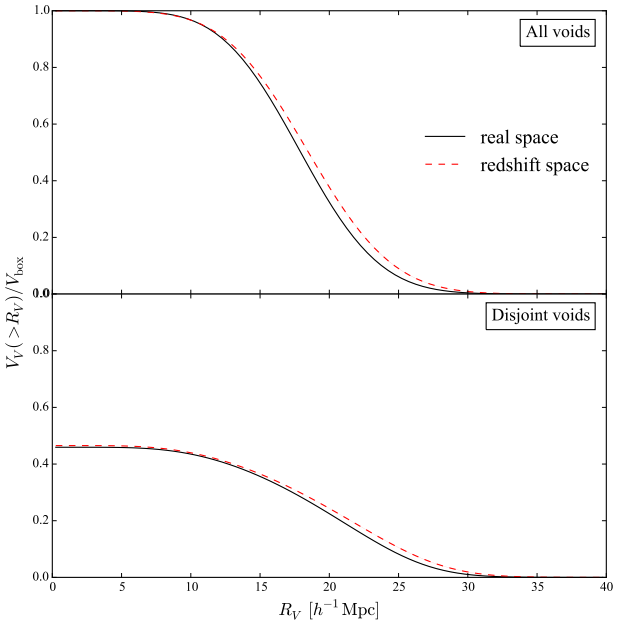

Figure 3. Volume filling fraction of *all voids* and *disjoint voids* both in real and in redshift space obtained from the mean over 100 PATCHY boxes (the 1-σ error bars are too tiny to be visible).

4 VOID PROPERTIES

In this section we present a thorough analysis of the resulting void catalogues obtained from applying DIVE to the PATCHY halo catalogues which permits us to obtain insights over the DT voids and properties of voids in general. We start with studying the void properties such as the volume filling function §4.1, the number function §4.2, and the spatial distribution of voids §4.3.

4.1 Volume filling fraction

Recent studies give very different Volume Filling Fractions (or cumulative volume function) of voids (e.g. Pan et al. 2012; Hoffman et al. 2012; Shandarin et al. 2012; Cautun et al. 2015), varying from about 60 % to more than 90 %. However, it is commonly agreed that voids occupy most of the volume of the Universe, as gravitational attraction causes over-densities to grow with time, resulting in the expansion of voids with cosmic evolution.

We then investigate the volume filling fraction from DT voids. For *disjoint voids* this is well-defined by computing the volume of the corresponding spheres. Nevertheless, it is not straightforward for *all voids*, due to the high overlapping fraction, as revealed in Fig. 2. In this case we use the volume of the associated tetrahedra as a proxy to incrementally compute the volume of the corresponding void regions.

We find that the overall volume of *all voids* reaches the total volume of the box, because the totality of tetrahedra fill the whole space (cf. Fig. 3). The volume function of DT voids reveals the volume occupied by empty regions that can at least fit a sphere with a given radius. The volume filling fraction of *disjoint voids* is much lower, covering slightly less than half of the total cubical volume considering down to the smallest voids, since cosmic empty regions are, in general, not spherical, especially at low redshifts.

Interestingly, for both species of voids, the volume filling fractions are higher in redshift space, especially at large R_V, because on large scales Redshift Space Distortions (RSD) squash the distribution of matter tracers along the line-of-sight, thus systematically expanding voids in an anisotropic way. RSDs on small scales, responsible for the Fingers-Of-God (FOG) effect, elongate clusters along the line of sight, hence reducing the volume of small voids. Towards small R_V, the volume filling fractions in real and redshift space are equal.

4.2 Number function

The number function (or abundance) is another fundamental property of voids. It dominates the statistical errors for the analyses, and is sensitive to the cosmological parameters (cf. e.g. Betancort-Rijo, Patiri, Prada & Romano 2009; Jennings, Li & Hu 2013) and the nature of dark energy (e.g. Cai, Padilla & Li 2015).

Since the DT voids are defined based on the matter tracers, the number function of voids are expected to be sensitive to the number density of haloes. To investigate this, we down-sample the 100 PATCHY mocks with halo number density of $3.5 \times 10^{-4}\,h^3\,\mathrm{Mpc}^{-3}$, and construct three more sets of PATCHY halo catalogues, with number density of $\{2, 2.5, 3\} \times 10^{-4}\,h^3\,\mathrm{Mpc}^{-3}$, respectively.

We find that the total number of voids N_V, shown as a function of radius R_V on the *left* panel of Fig. 4, significantly decreases for decreasing number densities. However, the number of large voids, together with the average radius of voids, increases. This indicates that there are two populations of voids with an opposite dependency on the number density of haloes, that can be separated by the void radius: one is correlated with the population of haloes, while the other is anti-correlated with the haloes.

A visualisation of the two types of populations of voids

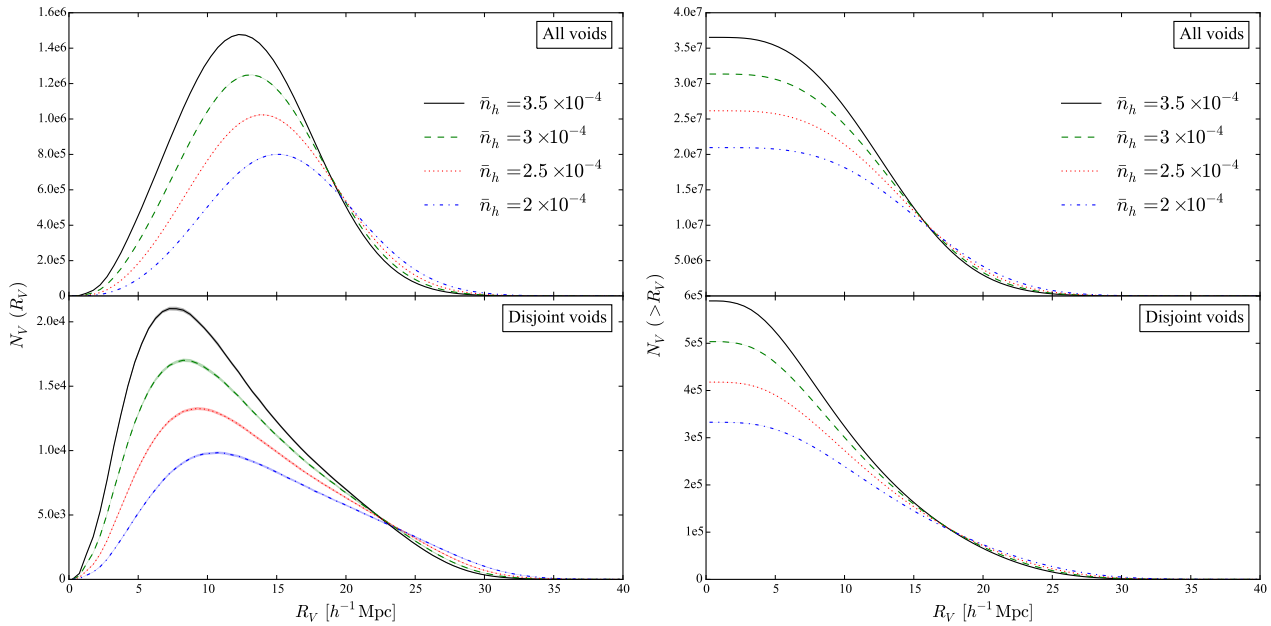

Figure 4. Number function (*left*) and cumulative number function (*right*) of voids resolved in halo catalogues with different halo number densities $\bar{n}_h$, in unit of $h^3\,\mathrm{Mpc}^{-3}$. (The 1-σ error bars are too tiny to be visible.)

can be found in Fig. 1. The *left* panel shows that the small voids are actually hosted in dense regions, while the *right* panel indicates that large voids are located in empty regions. These are representing the so-called *voids-in-clouds* and *voids-in-voids* classification of voids, as described in Sheth & van de Weygaert (2004), and are thus complementary tracers of the underlying density.

To separate the two classes of voids we consider the crossing point between the cumulative functions for varying halo number densities, as shown on the *right* panel of Fig. 4. From this we find that the transition from one class to the other occurs for void radii of about $R_V \geqslant 16$ and $17.5\,h^{-1}\mathrm{Mpc}$ for *all voids* and *disjoint voids*, respectively, which is not insensitive to the halo number densities. Interestingly, the transition radius for *all voids* is precisely the radius cut found to provide the optimal signal-to-noise ratio for the BAO signal from DT voids. Adding smaller radius contaminates the sample with *voids-in-clouds* with the opposite BAO signature (cf. Liang et al.).

The disjoint population has a larger fraction of small voids in general, while the critical radius for the two populations is slightly higher. The different number fraction between *all voids* and *disjoint voids*, shown in Fig. 5, indicates that voids with medium radius ($R_V \in [10, 20]\,h^{-1}\mathrm{Mpc}$) have high overlapping fractions in contrast to small voids ($R_V \leqslant 10\,h^{-1}\mathrm{Mpc}$).

The effect of RSDs in the halo distribution on the void number function is related to that for void volumes, and DIVE finds more voids with large radii (cf. Fig. 6). There is also a decrease in the number of voids with intermediate radii, presumably due to nonlinear RSDs (FOGs). For smaller voids with $R_V \sim 5\,h^{-1}\mathrm{Mpc}$, the number of voids increases again. This seems to be another effect of the *voids-in-clouds*. However, we should be cautious at this point, as the details of RSDs at small scales could have some systematic deviations from N-body simulation, since the PATCHY realisations rely on perturbation theory, and the PATCHY dark matter fields we rely have a resolution of $2.6\,h^{-1}\mathrm{Mpc}$.

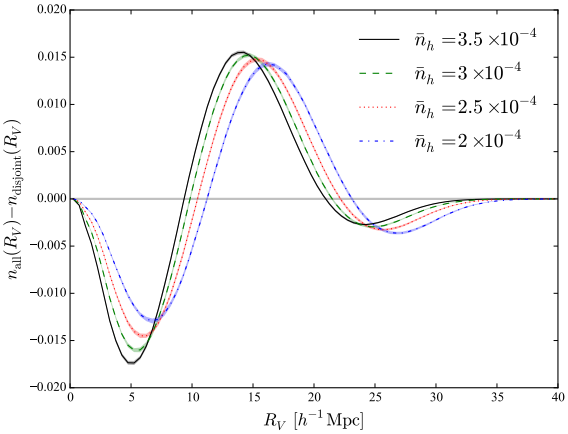
$\bar{n}_h = 3.5 \times 10^{-4}$
$\bar{n}_h = 3 \times 10^{-4}$
$\bar{n}_h = 2.5 \times 10^{-4}$
$\bar{n}_h = 2 \times 10^{-4}$
$n_{\mathrm{all}}(R_V) - n_{\mathrm{disjoint}}(R_V)$
$R_V\ [h^{-1}\mathrm{Mpc}]$

Figure 5. Difference of the number fraction between *all voids* and *disjoint voids* resolved in halo catalogues with different halo number densities $\bar{n}_h$ in units of $h^3\,\mathrm{Mpc}^{-3}$ represented by the corresponding lines. The shaded regions show the 1-σ errors obtained from 100 mocks with the corresponding colour-code.

To further explore the characteristics of the distribution of overlapping voids, we interpret the *disjoint voids* as parent voids (V_P), and overlapping voids as sub-voids (V_S). With these definitions we find that larger parent voids tend to have larger and more sub-voids (cf. Fig. 7). By changing the void definition from *disjoint voids* to *all voids* with large radii, we obtain more large voids in large empty regions, giving more weights to these regions.

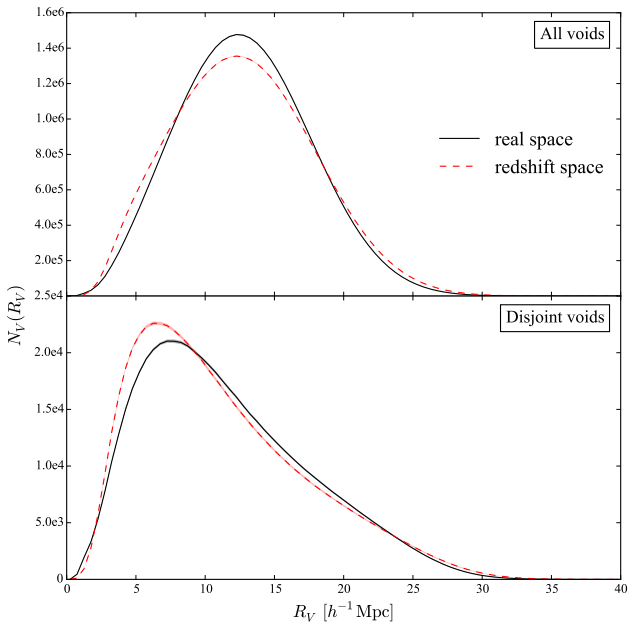

Figure 6. Number function of voids in real and redshift spaces. (The 1-σ error bars are too tiny to be visible.)

4.3 Spatial distribution of matter tracers and voids

In addition to the statistical description of the population of voids, we investigate the spatial distribution of voids. Fig. 8 (inspired by Hamaus et al. 2014a) presents the projected density field for different tracers extracted from a thin slice of one PATCHY realisation, where the normalised densities are shown: $\rho/\bar{\rho}$ or $n/\bar{n}$, where ρ and n denote the density and number density, respectively, and $\bar{\rho}$ and $\bar{n}$, indicate the average values across the whole volume.

The halo distribution follows the over-densities in the dark matter distribution, so does the number density field of DT voids. This indicates that the *voids-in-clouds* dominate the number density distribution, and is consistent with the number function shown in Fig. 4.

The *voids-in-voids* population of DT voids (*large* voids, with $R_V \geqslant 16\,h^{-1}$Mpc) is shown combined with the number density field of haloes with opposite signs at the *bottom* panel in Fig. 8. Haloes and *large* voids are clearly spatially separated, and together, fill the different regions of the cosmic web, forming a homogenous map. It indicates that the centres of *large* DT voids indeed trace the empty regions of the underlying density distribution, while small voids follow the distribution of dense regions. This claim needs however further quantitative verification, which we present below.

5 DARK MATTER DENSITY FIELD AROUND VOIDS

We present in a more quantitative way the environment in which the different classes of DT voids reside.

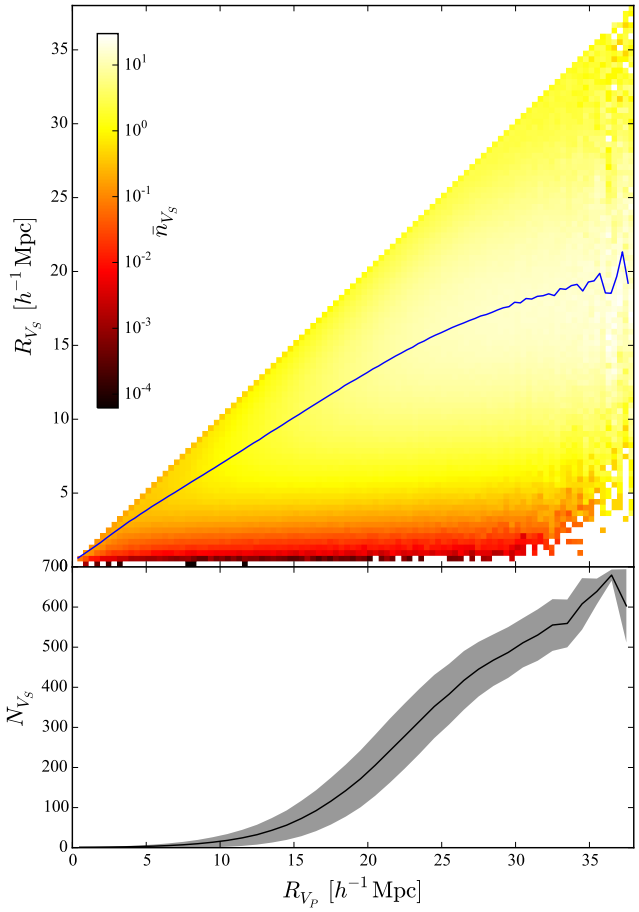

Figure 7. Radius and number distribution of sub-voids for different radius of the associated parent (distinct) voids. *Top*: for given radius of parent voids (V_P, or *disjoint voids*), the mean number fraction of sub-voids (V_S, or overlapping DT voids) of different radii. The blue curve represents the mean radius of sub-voids. *Bottom*: Number of sub-voids for different radii of parent voids. The shaded area shows the 1-σ errors obtained from all the parent voids in one realisation of PATCHY mocks.

5.1 Local dark matter density

The most direct cosmological environment information of the voids is given by the local dark matter density near the void centres. In order to explore the local environment of DT voids, we take the dark matter density field from PATCHY mocks, with the mesh size of about $2.6\,h^{-1}$Mpc (960^3 cells). The local dark matter density of each void is represented by the density of the closest cell.

The distribution of DT voids as a function of radius and local dark matter density (cf. Fig. 9) confirms that there are two void populations, one with large radii which reside in low density regions, and the other with small radii spread over the full density range.

The dispersion of the local dark matter density steadily decreases for increasing DT void radii. The majority of these voids are hosted in low density regions, and are hence tracing the empty regions with very low density. In contrast, the dispersion of the local density rapidly grows towards small DT void radii, reaching the typical density range for haloes. This indicates that the majority of small voids with $R_V < 5\,h^{-1}$Mpc are located in over-dense regions, and have a large

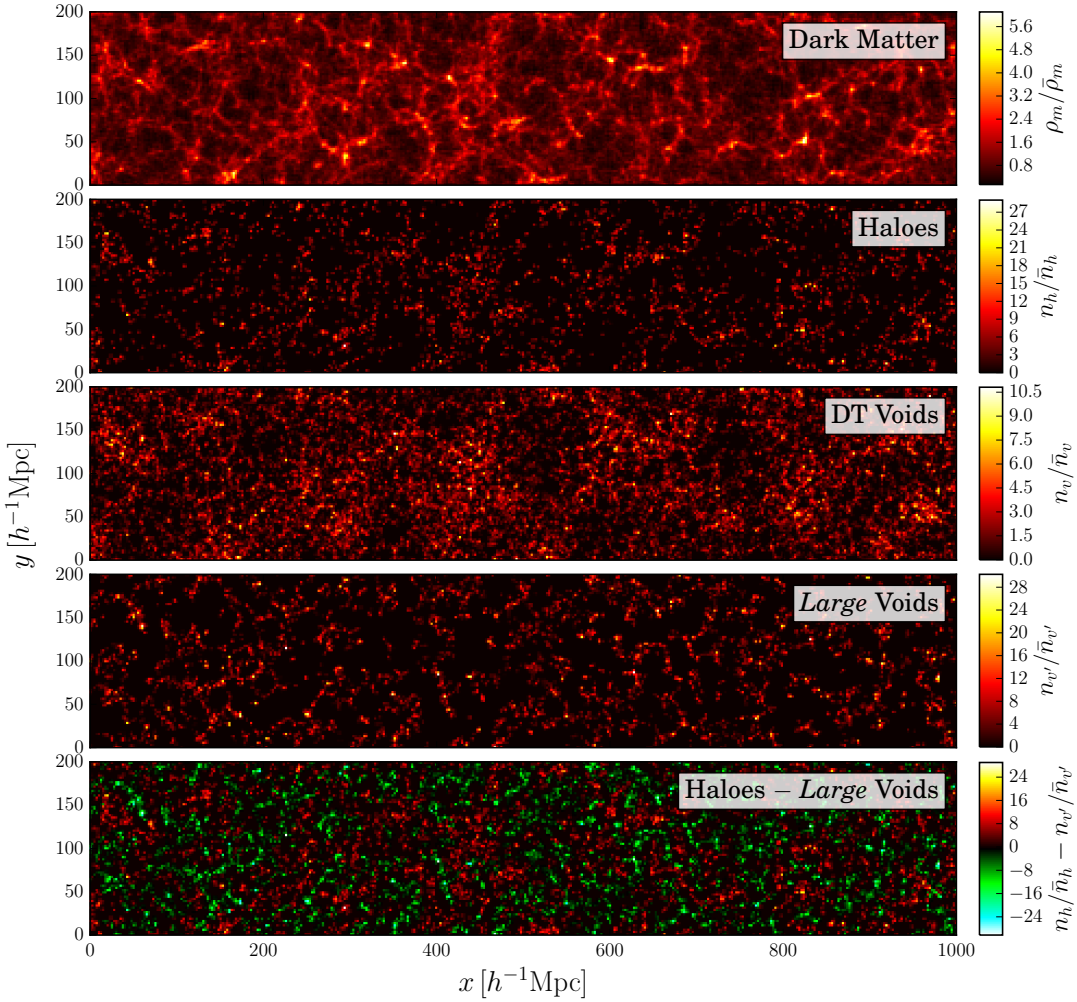

Figure 8. Projected density field for different tracers in a $1000 \times 500 \times 50\,h^{-3}\mathrm{Mpc}^3$ box extracted from one PATCHY realisation. *Large* Voids denote DT voids with $R_V \geqslant 16\,h^{-1}\mathrm{Mpc}$. Haloes − *Large* Voids indicate the combination of normalised number density of haloes and *large* voids, where the number density of voids is denoted by negative numbers.

bias. In particular, DT voids with $R_V \sim 4\,h^{-1}\mathrm{Mpc}$ have the same mean density as the haloes used to construct them.

5.2 Density profiles

The density profile of voids is a potentially powerful signature for constraining cosmological parameters and theories of gravity (e.g. Cai et al. 2015), although in practice it might be difficult to get precise measurements from observations. The universality of void density profiles has been discussed with many different methods and data (e.g. Colberg et al. 2005; Ricciardelli et al. 2013; Hamaus et al. 2014b; Nadathur et al. 2015). However, little attention has been paid to the intrinsic scatter of the density profiles. In general, void finders based on the reconstructed dark matter density field (e.g. ZOBOV and WVF) have relatively low errors (e.g. Hamaus et al. 2014b), while the fluctuations of the density profile from other void finders can be considerably large (e.g. Ricciardelli et al. 2013).

Since the DT voids number density is high (cf. § 4.2), it permits us to have reliable analyses for both the density profile and its fluctuations. Due to the limitation of the mesh resolution ($\sim 2.6\,h^{-1}\mathrm{Mpc}$) and the accuracy of the PATCHY dark matter density field, we select only relatively large DT voids and divide them into 5 classes according to the radius (cf. Fig. 10) for the density profile studies. Each class of voids, is further randomly partitioned into sub-samples that contain 2,000 voids. With one PATCHY realisation, the class with $R_V \geqslant 25\,h^{-1}\mathrm{Mpc}$ contains ∼140 sub-samples, while other classes with smaller radii have thousands of sub-samples. We then stack the voids in the sub-samples and compute the radial dark matter up to twice the void radius to obtain the density profile of DT voids.

We find that the shape of the DT void density profiles are in general close to the universal density profile presented in previous literature, however, our results show a stronger dependence on the radius (cf. Fig. 10). We further find that small voids, representing *voids-in-clouds*, can show positive density contrasts even near their centres. The profiles show a steep wall near the boundary of the voids, crossing zero over-density, and then, for larger radii, the density declines steadily towards the background value. For very large voids, we observe a similar rise in density. However, there is no zero over-density crossing close to the boundary. These uni-

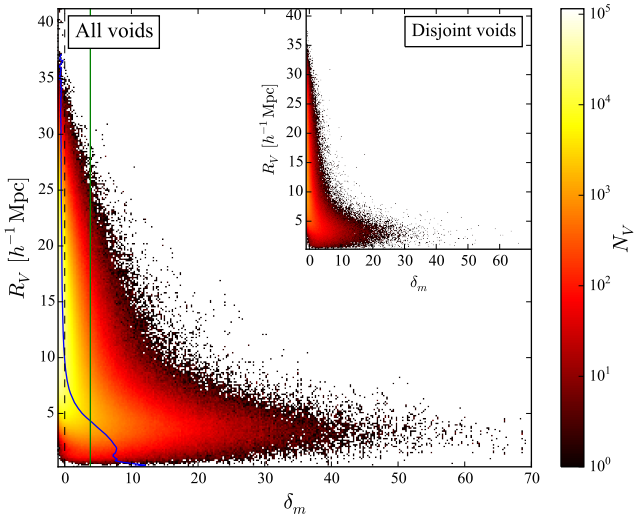

Figure 9. Number of DT voids with different radius (R_V) and local dark matter density contrast ($\delta_m \equiv \rho_m/\bar{\rho}_m - 1$). The blue curve stands for the mean DT voids density contrast as a function of radius, while the green line stands for the mean halo density contrast.

versal characteristics of void density profiles give a robust quantitative support to the initial claim that the centres of DT voids trace the emptiness of the universe. Furthermore, the volume covered by the distribution of DT voids is close to the voids defined by other sophisticated methods, based e.g. on the watershed approach.

Furthermore, the fluctuations of the density profiles normalised by the dark matter density ($\sigma_{\delta_m}/(1+\delta_m)$) also show an interesting universality, especially at small scales ($R_V \leqslant 10\,h^{-1}$Mpc). By combining the sub-samples, we find an intrinsic scatter of the density profile, which does not decrease with an increasing number of voids. The origin of this fluctuation is probably the background fluctuation level of the density field in under-dense regions. The *right* panel of Fig. 10 indicates an invariant behaviour of this intrinsic fluctuation. However, at scales close to the radius of the voids, such invariance is broken.

5.3 Cosmic web environment

The cosmic web is important to characterise the large scale structure and can be used to understand structure formation or test ΛCDM (e.g. Platen et al. 2011; Sousbie 2011; van de Weygaert et al. 2011; Shandarin et al. 2012; Nuza et al. 2014). So far we studied the relation between DT voids and the underlying dark matter density in a static perspective. We now use the dynamical cosmic web classification method introduced by Hahn et al. (2007) and Forero-Romero et al. (2009), in order to clarify the dynamical tidal field environment of DT voids, in which the cosmic web structures are classified into four types: knots, filaments, sheets, and voids. In brief, this method computes the tidal field tensor (T_{ij}) according to the density field (δ_m), i.e.,

$$T_{ij} = \frac{\partial^2 \phi}{\partial x_i \partial x_j}, \tag{3}$$

where ϕ is the gravitational potential, and is obtained through the Poisson equation:

$$\nabla^2 \phi = \delta_m. \tag{4}$$

Then we compare the three eigenvalues of T_{ij} with a given threshold ($\lambda_{\rm th}$). If all the three eigenvalues are above (below) $\lambda_{\rm th}$, then the local structure is collapsing (expanding) on all directions, forming a knot (void). When one (two) eigenvalue is above $\lambda_{\rm th}$, we have filament-like (sheet-like) structures.

In particular, we choose the $\lambda_{\rm th}$ parameter of 0.5 in this classification method, such that the volume filling fraction of the four cosmic web types (knots, filaments, sheets, and voids) are about 0.6 %, 7.6 %, 27.8 %, and 64.0 % respectively (i.e. with a void VFF > 60%). We then classify the DT voids according to the position of their centres (see Fig. 11). For $R_V \geqslant 15\,h^{-1}$Mpc, over 80 % of the DT voids are in the void-like type, and more than 95 % of the DT voids are in either void-like or sheet-like structures, where the space is expanding on at least two directions, thus further confirming that the *voids-in-voids* class of DT voids is following the emptiness.

As the void radius decreases, the DT void fraction in sheets, filaments, and knots display maxima at different sizes, and the highest occupation structure varies from voids to sheets, and then to filaments. The evolution of the DT void fraction indicates that the characteristic scale of the four cosmic web structures (voids, sheets, filaments, and knots) decreases in respective order. In particular, the void population in filamentary structures shows a maximum at $R_V \sim 3.5\,h^{-1}$Mpc, which is consistent with the typical separation of galaxies along filaments ($\sim 7\,h^{-1}$Mpc) obtained from the correlation function of galaxies in filaments (Tempel et al. 2014). The position of the peaks in Fig. 11 reveals the typical separation of haloes in different types of cosmic web structures, since small DT voids connect four haloes with a maximum separation of $2R_V$.

6 VOID CLUSTERING

Due to the large volume of voids, they are typically regarded as rare objects in the universe. Therefore, the clustering properties of DT voids are seldom studied (cf. however Chan et al. 2014; Clampitt et al. 2015). However, the large number of DT voids permits us to have reliable clustering statistics, such as power spectra, or correlation functions. We present here some results on power spectra.

6.1 Auto and cross power spectra

As we have presented in previous sections, there are two completely different populations of DT voids, i.e., *voids-in-voids* and *voids-in-clouds* respectively. Therefore, instead of considering the whole void sample, let us consider the two populations separately. Following § 4.2, we define *large* voids as $R_V \geqslant 16\,h^{-1}$Mpc voids. Similarly, we also define *small* voids as $R_V < 8\,h^{-1}$Mpc, following the local densities shown in Fig. 9 and the cosmic web types in Fig. 11.

We present the auto and cross power spectra for different tracers (dark matter, haloes, *large* DT voids, and *small* DT voids) based on 100 PATCHY mocks in Fig. 12, where we adopt the Cloud-In-Cell (CIC) particle mass assignment

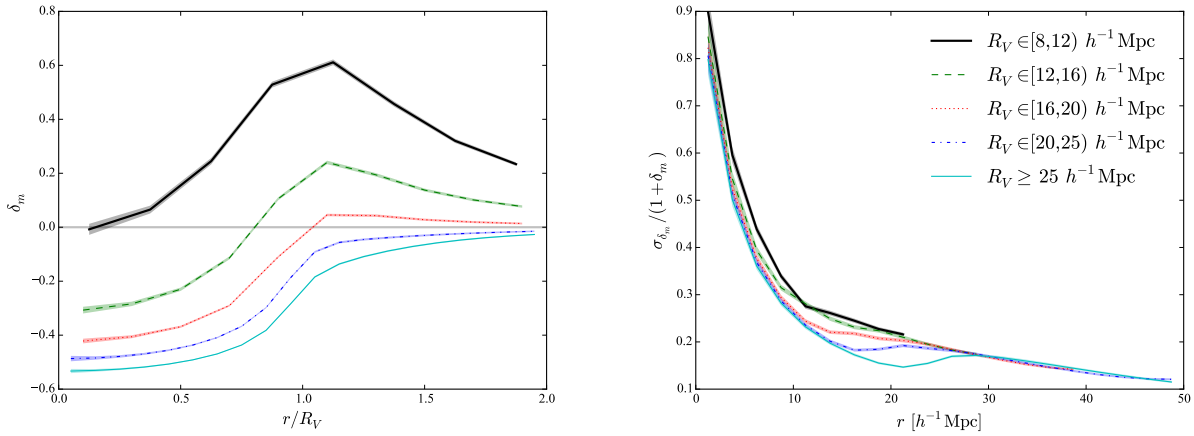

Figure 10. Mean density profile (*left*) and the standard deviation of the density profile (*right*) of DT voids, where r is the distance to the centre of the void. The shaded regions show the 1-σ errors obtained with sub-samples.

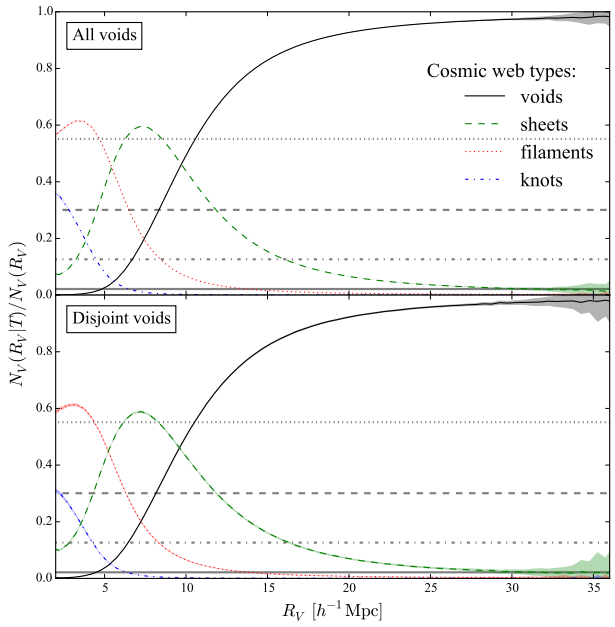

Figure 11. Fraction of DT void centres for different cosmic web types (T) defined in a dynamical way. The thick grey lines denote the fraction of haloes in different cosmic web types. The shaded regions show the 1-σ errors obtained from 100 mocks.

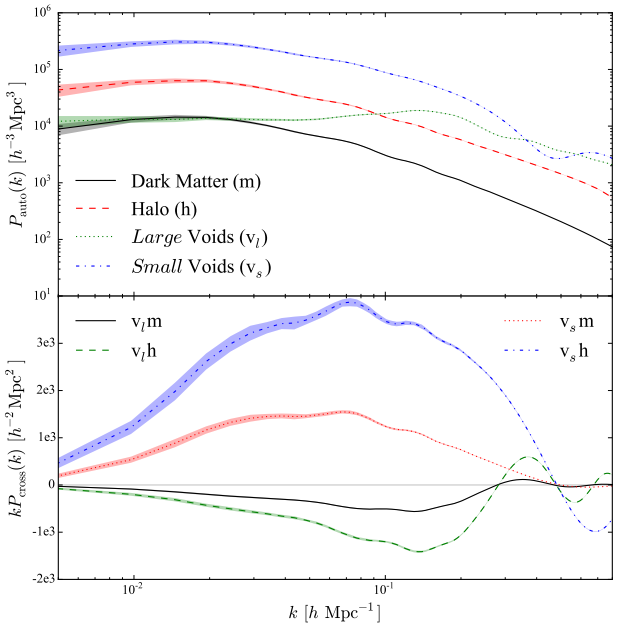

Figure 12. Auto and cross power spectra for different tracers based on the PATCHY mocks. The shaded regions show the 1-σ errors from 100 mocks.

scheme with a grid size of 960^3 to perform fast Fourier Transform, and take into account the aliasing and shot noise corrections (cf. Jing 2005).

The two classes (*small* and *large* voids) show distinct power spectra, reflecting their different biases. The *large* voids show a relatively low bias, and the amplitude of the auto power spectrum at small k is very close to that of dark matter. On the contrary, the bias of the *small* voids is fairly large, and the auto power spectrum of this class of voids follows the halo power spectrum quite well up to $k \sim 0.1\,h\,\mathrm{Mpc}^{-1}$. This is because DIVE selects groups of four haloes with a maximum separation, and works like the first phase of the cluster finding scheme developed by Marinoni et al. (2002). In this case, we are likely to find gravitational bound systems of haloes, which should have a higher bias than the overall population of haloes.

Moreover, there are dips and oscillations at large k ($k > 0.1\,h\,\mathrm{Mpc}^{-1}$) for the auto and power spectra respectively, indicating patterns similar to the halo exclusion effect (Baldauf et al. 2013) and void exclusion effect (Chan et al. 2014). Therefore, even though the overlapping fraction is fairly high for the DT voids, there are still strong exclusion effects. This effect can be recognised also from the density profile shown in § 5.2, where the profile is steep inside the voids, and implies a clear exclusion from other voids.

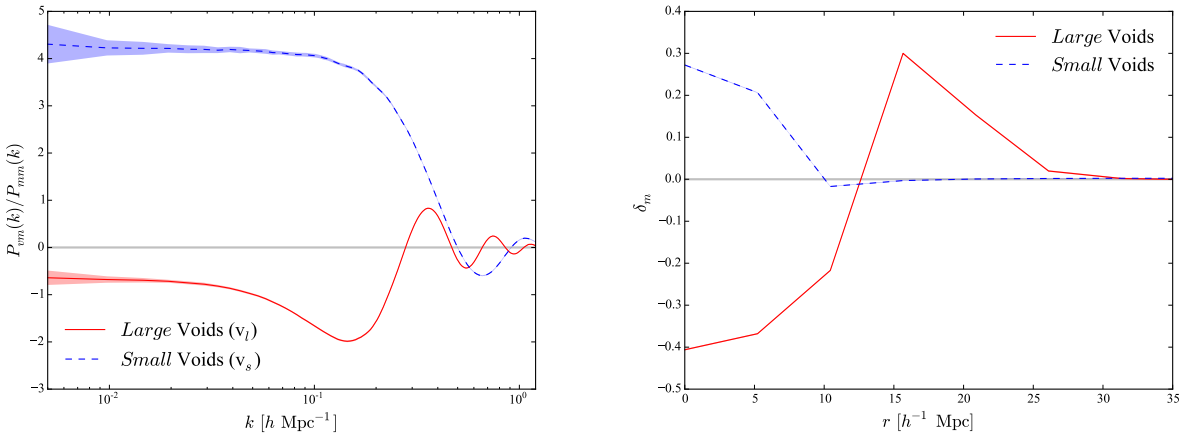

Figure 13. Bias (*left*) and radial density profile (*right*) of DT voids, obtained from the auto and cross power spectra. The shaded regions show the 1-σ errors from 100 mocks.

6.2 Void bias and density profile

The clustering statistics permits us to have a quantitative measurement of the bias. Since voids suffer less from late-time nonlinear effects (van de Weygaert & van Kampen 1993), we adopt the linear estimator of the scale-dependent bias of voids with respect to dark matter ($b_m(k)$):

$$b_m(k) = \frac{P_{vm}(k)}{P_{mm}(k)}, \tag{5}$$

where $P_{vm}(k)$ indicates the cross power spectrum between voids and dark matter, and $P_{mm}(k)$ is the auto power spectrum of dark matter.

We present the bias for the two classes of DT voids (*large* and *small* voids) on the *left* panel of Fig. 13. In the linear regime (small k), the bias is nearly constant, but the two classes clearly show two distinct biases. The *large* voids have a negative dark matter bias of about -0.7, indicating a very low density environment, while the bias of the *small* voids is around 4.2, about twice the bias of LRGs (Tegmark et al. 2006).

The radial density profile of the stacked voids describes the cross correlation between dark matter and void centres, thus the cross bias between dark matter and voids is essentially the Fourier counterpart of the density profile neglecting the shot noise (Chan et al. 2014; Hamaus et al. 2014a):

$$u_v(k) = \frac{P_{vm}(k)}{P_{mm}(k)} \times \left|\frac{P_{mm}(k)}{P_{vm}(k)}\right|_{k\to 0}, \tag{6}$$

where $u_v(k)$ is the void density profile in Fourier space. This equation is valid, since our dark matter samples is large enough ($\bar{n}_m^{-1} \ll P_{mm}(k)$). We are then able to reproduce the density profile of the two classes of voids using the Fourier Transform of the scale-dependent bias.

The *right* panel of Fig. 13 shows the density profile obtained from the cross power spectra of 100 PATCHY mocks. The *large* voids show a typical void density profile, while the *small* void class show a very different one, in which the density contrast in the central part is very high. This confirms that the small radius voids found by DIVE are essentially groups of haloes.

7 CONCLUSIONS

We have presented a new parameter-free cosmological void finder based on Delaunay Triangulation, which emerges as the natural approach to be applied to discrete samples of haloes or galaxies. This method is very efficient on large data sets and we plan to use it for upcoming galaxy redshift surveys. In particular, the speed of the Delaunay Triangulation algorithm allows us to find the voids from catalogues with millions of objects covering huge volumes within minutes.

The complete set of Delaunay Triangulation voids (DT voids) shows high overlapping fractions, and cannot be considered as individual spherical under-dense regions in the universe. Interestingly their distribution depicts the aspherical shape of cosmic voids serving as proxies for the emptiness in the Universe. With this void definition, the number of voids is about 7 times the halo population with a number density of $3.5 \times 10^{-4}\, h^3\mathrm{Mpc}^{-3}$, which permits us to perform reliable statistical studies, in particular clustering analysis, based on voids. Besides, the associated tetrahedra of DT voids constraint by Delaunay Triangulation involve high order correlation of the tracers, which allows us to extract additional information from distribution of galaxies when computing the correlation function of voids (cf. Kitaura et al., Liang et al.). The cosmological gain of DT voids will be discussed in a future paper (Chuang et al., in preparation).

We further studied the DT voids in a hierarchical perspective, where we interpret the maximum non-overlapping spheres as parent (disjoint) voids, and the overlapping ones as sub-voids, showing that the *disjoint voids* alone are not able to represent all the under-dense regions of the universe, due to their low volume filling fraction. Moreover, we find that the larger parent voids have more and larger sub-voids.

Furthermore, we show that there exist two distinct populations of DT voids, i.e., *voids-in-voids* and *voids-in-clouds*, which can be accurately separated from each other based on the radius of the spheres. Some of the properties we have found for the two void populations are:

(i) The volume filling fractions and number functions have different responses to the halo Redshift Space Distortion effects.

(ii) The number function of DT voids is strongly correlated with the number density of tracers. However, small voids follow the population of tracers, while the number of large voids is anti-correlated with the tracer number density. Moreover, the halo and the large void number density fields are complementary to each other across cosmic volumes.

(iii) The dark matter environment of the two species of voids are different. The centres of large voids are mostly in under-dense regions, which is consistent with the voids defined from the dark matter density field in a dynamical way. While the centres of small voids are in very dense regions, and only a small fraction is defined as voids using the dynamical method. Similarly, the density profile of large voids are deeper in the centre, while the small voids have relatively high centre density, as well as a high wall near the boundary.

(iv) We find from clustering statistics that the two void populations have different bias. Large voids have negative bias, and small voids have high positive bias.

We confirmed that the large DT voids (*voids-in-voids*) follow the under-dense regions of the universe, while the small voids (*voids-in-clouds*) are essentially groups of the tracers, which are gravitational bound systems efficiently found by DIVE. We find also an universal intrinsic fluctuation of the void density profile, which may be related to the density fluctuation of the underlying dark matter field.

We apply this technique for further studies of voids in the large scale structure, to constrain cosmological parameters and alternative models of gravity. The BAO analyses of the two point correlation functions are detailed in accompanying papers (Kitaura et al., Liang et al., Chuang et al.), and the work on the power spectra is in preparation. Furthermore, Hamaus et al. (2014a) present a novel scale found by void-galaxy cross correlation, and we are studying this characteristic scale using DT voids in the BOSS galaxy data.

ACKNOWLEDGMENTS

CZ thanks He Wang and Qing Shu for some instructive discussions on the Delaunay Triangulation. CZ, CT, and YL acknowledge support from Tsinghua University, and 985 program. FSK thanks support from the Leibniz Society for the Karl-Schwarzschild fellowship.

We acknowledge the EREBOS/THEIA/GERAS clusters at AIP and the HYDRA HPC-cluster of IFT-UAM/CSIC for the computations. Fig. 1 and Fig. 2 are made by the WOLFRAM MATHEMATICA[3] software.

REFERENCES

Abel T., Hahn O., Kaehler R., 2012, MNRAS, 427, 61
Aikio J., Mähönen P., 1998, ApJ, 497, 534
Aragón-Calvo M. A., Jones B. J. T., van de Weygaert R., van der Hulst J. M., 2007, A&A, 474, 315
Baldauf T., Seljak U., Smith R. E., Hamaus N., Desjacques V., 2013, Phys. Rev. D, 88, 083507
Bergé J., Price S., Amara A., Rhodes J., 2012, MNRAS, 419, 2356
Bernardeau F., 1996, in Coles P., Martinez V., Pons-Borderia M.-J., eds, Astronomical Society of the Pacific Conference Series Vol. 94, Mapping, Measuring, and Modelling the Universe. p. 253 (arXiv:astro-ph/9601083)
Betancort-Rijo J., Patiri S. G., Prada F., Romano A. E., 2009, MNRAS, 400, 1835
Braun J., Thieulot C., Fullsack P., DeKool M., Beaumont C., Huismans R., 2008, Physics of the Earth and Planetary Interiors, 171, 76
Brönnimann H., Fabri A., Giezeman G.-J., Hert S., Hoffmann M., Kettner L., Pion S., Schirra S., 2015, in , CGAL User and Reference Manual, 4.6.3 edn, CGAL Editorial Board, http://doc.cgal.org/4.6.3/Manual/packages.html#PkgKernel23Summary
Brunino R., Trujillo I., Pearce F. R., Thomas P. A., 2007, MNRAS, 375, 184
Cai Y.-C., Padilla N., Li B., 2015, MNRAS, 451, 1036
Cardiel N., Jiménez-Esteban F. M., Alacid J. M., Solano E., Aberasturi M., 2011, MNRAS, 417, 3061
Cautun M., van de Weygaert R., Jones B. J. T., 2013, MNRAS, 429, 1286
Cautun M., van de Weygaert R., Jones B. J. T., Frenk C. S., 2015, preprint (arXiv:1501.01306)
Cedrés B., Cepa J., Bongiovanni Á., Castañeda H., Sánchez-Portal M., Tomita A., 2012, A&A, 545, A43
Chan K. C., Hamaus N., Desjacques V., 2014, Phys. Rev. D, 90, 103521
Chuang C.-H., et al., 2015, MNRAS, 452, 686
Clampitt J., Jain B., Sánchez C., 2015, preprint (arXiv:1507.08031)
Colberg J. M., Sheth R. K., Diaferio A., Gao L., Yoshida N., 2005, MNRAS, 360, 216
Dawson K. S., et al., 2013, AJ, 145, 10
Delaunay B., 1934, Izv. Akad. Nauk SSSR, Otdelenie Matematicheskii i Estestvennyka Nauk, 7, 1
Eisenstein D. J., et al., 2011, AJ, 142, 72
El-Ad H., Piran T., 1997, ApJ, 491, 421
Falck B. L., Neyrinck M. C., Szalay A. S., 2012, ApJ, 754, 126
Forero-Romero J. E., Hoffman Y., Gottlöber S., Klypin A., Yepes G., 2009, MNRAS, 396, 1815
Foster C., Nelson L. A., 2009, ApJ, 699, 1252
Hahn O., Porciani C., Carollo C. M., Dekel A., 2007, MNRAS, 375, 489
Hamaus N., Wandelt B. D., Sutter P. M., Lavaux G., Warren M. S., 2014a, Physical Review Letters, 112, 041304
Hamaus N., Sutter P. M., Wandelt B. D., 2014b, Physical Review Letters, 112, 251302
Hoffman Y., Metuki O., Yepes G., Gottlöber S., Forero-Romero J. E., Libeskind N. I., Knebe A., 2012, MNRAS, 425, 2049
Hoyle F., Vogeley M. S., 2002, ApJ, 566, 641
Icke V., van de Weygaert R., 1987, A&A, 184, 16
Jamin C., Pion S., Teillaud M., 2015, in , CGAL User and Reference Manual, 4.6.3 edn, CGAL Editorial Board, http://doc.cgal.org/4.6.3/Manual/packages.html#PkgTriangulation3Summary
Jennings E., 2012, MNRAS, 427, L25
Jennings E., Li Y., Hu W., 2013, MNRAS, 434, 2167
Jing Y. P., 2005, ApJ, 620, 559
Kitaura F.-S., Heß S., 2013, MNRAS, 435, L78
Kitaura F.-S., Yepes G., Prada F., 2014, MNRAS, 439, L21
Kitaura F.-S., et al., 2015a, preprint (arXiv:1509.06400)
Kitaura F.-S., Gil-Marín H., Scóccola C. G., Chuang C.-H., Müller V., Yepes G., Prada F., 2015b, MNRAS, 450, 1836
Klypin A., Yepes G., Gottlober S., Prada F., Hess S., 2014, preprint (arXiv:1411.4001)
Lang M., Holley-Bockelmann K., Sinha M., 2015, ApJ, 811, 152
Lee J., Park D., 2009, ApJ, 696, L10
Marinoni C., Davis M., Newman J. A., Coil A. L., 2002, ApJ,

[3] http://www.wolfram.com/mathematica/

580, 122
Medek P., Beneš P., Sochor J., 2007, Journal of WSCG, 15, 107
Nadathur S., Hotchkiss S., Diego J. M., Iliev I. T., Gottlöber S., Watson W. A., Yepes G., 2015, MNRAS, 449, 3997
Neyrinck M. C., 2008, MNRAS, 386, 2101
Nuza S. E., Kitaura F.-S., Heß S., Libeskind N. I., Müller V., 2014, MNRAS, 445, 988
Padilla N. D., Ceccarelli L., Lambas D. G., 2005, MNRAS, 363, 977
Pál A., Bakos G. Á., 2006, PASP, 118, 1474
Pan D. C., Vogeley M. S., Hoyle F., Choi Y.-Y., Park C., 2012, MNRAS, 421, 926
Patiri S. G., Betancort-Rijo J. E., Prada F., Klypin A., Gottlöber S., 2006, MNRAS, 369, 335
Platen E., van de Weygaert R., Jones B. J. T., 2007, MNRAS, 380, 551
Platen E., van de Weygaert R., Jones B. J. T., Vegter G., Calvo M. A. A., 2011, MNRAS, 416, 2494
Ricciardelli E., Quilis V., Planelles S., 2013, MNRAS, 434, 1192
Rodríguez-Torres S. A., et al., 2015, preprint (arXiv:1509.06404)
Romano-Díaz E., van de Weygaert R., 2007, MNRAS, 382, 2
Schaap W. E., van de Weygaert R., 2000, A&A, 363, L29
Shandarin S., Feldman H. A., Heitmann K., Habib S., 2006, MNRAS, 367, 1629
Shandarin S., Habib S., Heitmann K., 2012, Phys. Rev. D, 85, 083005
Sheth R. K., van de Weygaert R., 2004, MNRAS, 350, 517
Song H., Lee J., 2009, ApJ, 701, L25
Sousbie T., 2011, MNRAS, 414, 350
Springel V., 2010, MNRAS, 401, 791
Sutter P. M., Pisani A., Wandelt B. D., Weinberg D. H., 2014, MNRAS, 443, 2983
Tegmark M., et al., 2006, Phys. Rev. D, 74, 123507
Tempel E., Kipper R., Saar E., Bussov M., Hektor A., Pelt J., 2014, A&A, 572, A8
Trujillo I., Carretero C., Patiri S. G., 2006, ApJ, 640, L111
Zhao C., Kitaura F.-S., Chuang C.-H., Prada F., Yepes G., Tao C., 2015, MNRAS, 451, 4266
van de Weygaert R., Schaap W., 2007, preprint (arXiv:0708.1441)
van de Weygaert R., van Kampen E., 1993, MNRAS, 263, 481
van de Weygaert R., et al., 2011, preprint (arXiv:1110.5528)

This paper has been typeset from a TEX/LATEX file prepared by the author.